*Progress In Electromagnetics Research B, Vol. 19, 385–403, 2010*

# EFFECTS OF GEOMETRY ON AMPLIFICATION PROPERTY OF ERBIUM DOPED HOLEY FIBER AMPLIFIERS USING SCALAR EFFECTIVE INDEX METHOD

**M. Karimi**

Physics Group
Razi University
Kermanshah, Iran

**F. E. Seraji**

Optical Communication Group
Iran Telecom Research Center
Tehran, Iran

**Abstract**—Holey fibers (HF) with their peculiar properties have been used in fabrication of Erbium doped holey fiber amplifiers (EDHFA) for third optical communication window. In this paper, by using scalar effective index method, the analyses are presented to investigate the effects of HF geometrical parameters on the gain performance of the EDHFAs. The hierarchical variations of the parameters, including the air-hole sizes (AHS), propagating modes of the core and cladding, mode field diameter of the signal and pump, would cause alterations in the maximum gain and the optimum lengths of the EDHFAs. By determining the normalized frequency of the HF in wide range variations of the air-hole diameter, air-hole spacing, and air-filling factor (AFF), the single-mode regions for signal and pump wavelengths are obtained, where the maximum gain and the optimum lengths are evaluated. In addition, the influence of pump power and the dopant concentration in terms of the AFF are investigated. It is shown that by using suitable AHS and AFF, one can obtain a higher gain for a shorter optimum length in the EDHFAs.

The obtained results can be a useful tool for design of HF-based optical amplifiers with lesser effects of amplified spontaneous emission and nonlinearities because of shorter optimized length.

Corresponding author: F. E. Seraji (feseraji@itrc.ac.ir).

## 1. INTRODUCTION

In recent years photonic crystal fibers (PCFs) have emerged as an attractive alternative to solve many problems of conventional optical fibers. The PCFs can be classified in two categories according to their wave-guiding principle. The first one, index-guiding micro structured fibers (MF) or holey fibers (HF) which guide light in the same way as standard optical fibers [1], based on total internal reflection (TIR) [2]; and the second one, photonic band gap fibers (PBF) where the light propagation is confined through the band gap effect [3]. The main parameter of these fibers, such as numerical aperture, mode areas, group velocity dispersion (GVD), can change by altering the holes structures and sizes in the cladding. The flexibility of main parameters in the HF has led to the development of several applications in the fields of optical communications [4, 5], nonlinear optics [6], sensing [7], high power technology [8], dispersion tailored fibers [9], optical metrology [10], optical filters [11], and active fibers [12]. Narrow-core HFs have been widely applied in nonlinear optics, e.g., in super continuum generation and parametric amplification due to their enhanced nonlinearity [13, 14]. Large-core, endlessly single-mode HFs with high numerical aperture have been developed for applications in telecommunications and high optical power delivery [15].

Numerical simulations play an important role for the design and modeling of optical components. To simulate optical component based on HFs, the utilized HFs should be analyzed with one of the reported techniques [16]. Combining effective index model with rate equation is simple and fast model to analyze Erbium doped holey fiber amplifiers (EDHFAs) [17]. In the reported works, hole-assisted Erbium-doped amplifiers [18], honeycomb and cobweb photonic crystal fiber [19] large-mode area double-cladding HFs [20], have been studied with finite element method (FEM). Although FEM have more accuracy to analyze the EDHFAs with different hole geometries, it is a more time consuming method than other simple method such as effective index method (EIM). In Ref. [18], the variations of refractive index and hence the gain of EDHFAs at air-hole pitch $\Lambda = 4\,\mu\text{m}$ for three different air-filling factor (AFF) $d/\Lambda$ are reported using FEM, where $d$ is the air-hole size (AHS).

The simulation results of the EDHFA using fundamental space filling mode have good agreement with the experimental results [17, 21]. In the present paper, the effects of geometry on amplification property of EDHFAs with periodic air-hole arrangement in the cladding are analyzed using scalar effective index method (SEIM). A brief introduction to the numerical model applied in this work is reported in

the next section. In the simulation and analysis section, variations of the effective index and mode-field diameter (MFD) by changing hole geometry of a honeycomb lattice is determined. By using obtained results, the single-mode region by AHS and AFF is obtained in the EDHFA's doped with 6% Germanium dopant.

The variations of maximum gain and optimum length are determined in single-mode regions. This paper by using doped HF presents design of an amplifier with improved properties. We will show that when using the signal and the pump wavelengths in the single-mode region of the EDHFA, one can enhance the maximum gain of the amplifier with a lower pump powers.

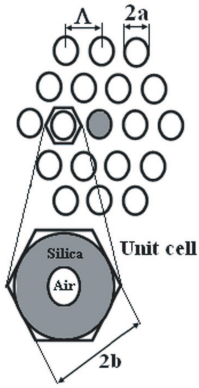


**Figure 1.** Hexagonal unit cell in the cladding with air hole of radius $a$ and silica radius of $b$.

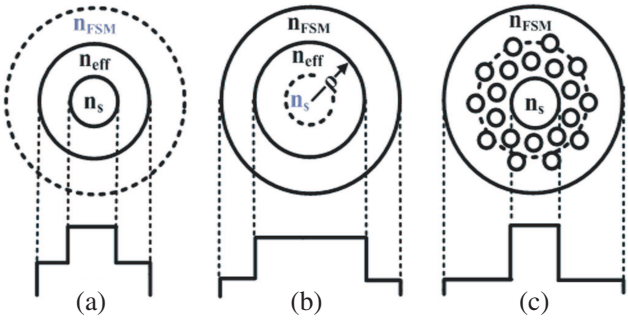


**Figure 2.** Development of equivalent step index fiber for the HF.

## 2. ERBIUM DOPED HOLEY FIBER MODELING

In modeling HFs by EIM, effective refractive index of cladding is replaced by average refractive index of fundamental space filling mode $n_{FSM} = \beta_{FSM}/k_0$ where $\beta_{FSM}$ is the space filling mode propagation constant, $k_0 = 2\pi/\lambda_0$ wave number in free space, and $\lambda_0$ is free space wavelength. The value of $n_{FSM}$ is evaluated by solving the scalar wave equation within a unit cell in the cladding of the HF in Fig. 1 as follows [22, 23]:

$$\begin{aligned} \Psi &= AI_0(WR); \quad R = r/a \quad \text{(within air-hole)} \\ &= BJ_0(RU) + CY_0(RU) \quad \text{(within silica region)} \end{aligned} \tag{1}$$

where $a$ is air-hole radius, $r$ is cylindrical parameter of the fiber, $Y_0$, $J_0$, and $I_0$ are Bessel functions. By inserting boundary condition in fundamental mode we obtain the eigenvalue equation as:

$$BJ_1(u) + CY_1(u) = 0 \tag{2}$$

Using Bessel functions $I_0$, $I_1$, $J_0$, $J_1$, $Y_0$, and $Y_1$, the constants $A$, $B$, and $C$ are determined by

$$\begin{aligned} AWI_1(W) &= -\frac{A}{J_0(U)}\left[I_0(W) - \frac{C}{A}Y_0(U)\right] - CUY_1(U) \\ C &= \frac{A\left[WI_1(W)J_0(U) + UJ_1(U)I_0(W)\right]}{U\left[J_1(U)Y_0(U) - J_0(U)Y_1(U)\right]} \\ B &= \frac{A}{J_0(U)}\left[I_0(W) - \frac{Y_0(U)\left[WI_1(W)J_0(U) + UJ_1(U)I_0(W)\right]}{U\left[J_1(U)Y_0(U) - J_0(U)Y_1(U)\right]}\right] \end{aligned} \tag{3}$$

In Eq. (3) the parameters $U$, $W$, and $u$ are defined as follows:

$$\begin{aligned} U &= k_0\, a\sqrt{n_s^2 - n_{FSM}^2} \\ W &= k_0\, a\sqrt{n_{FSM}^2 - n_a^2} \\ u &= k_0\, b\sqrt{n_s^2 - n_{FSM}^2} \end{aligned} \tag{4}$$

where $b = \Lambda(\sqrt{3}/2\pi)^{0.5} \approx 0.525\Lambda$ is radius of hexagonal unit cell [24], $n_s$ and $n_a$ are refractive indices of pure silica and air, respectively.

Now to determine the parameters in Eq. (4), we replace the HF with an equivalent step index fiber (ESIF) with core radius of $\rho$ in three steps (a), (b), and (c) as shown in Fig. 2. The solution of fundamental mode for the equivalent structure of Fig. 2(c) from Eq. (1) is given as

$$\begin{aligned} \Psi &= AI_0(U_{eff}R); \quad R < 1 \\ &= BJ_0(W_{eff}R) \quad R > 1 \end{aligned} \tag{5}$$

where the corresponding effective HF parameters are redefined as

$$\begin{aligned} U_{eff} &= k_0\rho\sqrt{n_{\text{core}}^2 - n_{eff}^2} \\ W_{eff} &= k_0\,\rho\sqrt{n_{eff}^2 - n_{FSM}^2} \\ V_{eff} &= k_0\,\rho\sqrt{n_{\text{core}}^2 - n_{FSM}^2} \end{aligned} \tag{6}$$

where $n_s$ is replaced by $n_{\text{core}}$ for refractive index of the core.

We define an ESIF with the core radius $\rho = 0.64\Lambda$, and corresponding core refractive index of $n_{\text{core}}$ (for $r \le \rho$) and $n_{FSM}$ (for $r > \rho$). The electric field component $E_x$ of the fundamental mode in the corresponding regions are [17, 25]:

$$E_x = \begin{cases} \frac{E_0 J_0\left(U_{eff} r/\rho\right)}{J_0\left(U_{eff}\right)} & r \le \rho \\ \frac{E_0 K_0\left(W_{eff} r/\rho\right)}{K_0\left(W_{eff}\right)} & r > \rho \end{cases} \tag{7}$$

The boundary condition is [26]:

$$\frac{J_0(U_{eff})}{U_{eff} J_1(U_{eff})} = \frac{K_0(W_{eff})}{W_{eff} K_1(W_{eff})} \tag{8}$$

where $K_0$ and $K_1$ are zero and first order modified Bessel functions respectively. Using $n_{FSM}$ in Eq. (8) the value of $n_{eff}$ can be obtained numerically. The refractive index of core $n_{\text{core}}$ is obtained from Sellemier equation for $GeO_2/SiO_2$ glass for whole wavelength region as [18]:

$$n_s^2 = 1 + \sum_{i=1}^{3} \frac{\left[SA_i + x\left(GA_i - SA_i\right)\right]\lambda_0^2}{\lambda_0^2 - \left[SL_i + x\left(GL_i - SL_i\right)\right]^2} \tag{9}$$

where $x$ is molar fraction of $GeO_2$ and $SA_i$, $SL_i$, $GA_i$, and $GL_i$ are coefficients of Sellemier equation for $SiO_2$ and $GeO_2$ glasses, respectively [18], $\lambda_0$ is free space wavelength in micrometer. In the following calculations, for the proper mode guidance and optimized operation of the EDHF with better dependency on fiber geometry, the value of $x$ is taken as 6% [18].

The intensity pattern $\Psi(r, \Omega)$, proportional to $|E_x|^2$ can be approximated as a Gaussian envelop function as:

$$\psi\left(r, \Omega\right) = \frac{e^{-r^2/\Omega^2}}{\pi\Omega^2} \tag{10}$$

where the effective MFD ($\Omega$) for core mode $LP_{01}$, is defined as [17, 27]:

$$\Omega_{eff} = \rho\, J_0\left(U_{eff}\right) \frac{V_{eff}}{U_{eff}} \frac{K_1\left(W_{eff}\right)}{K_0\left(W_{eff}\right)} \tag{11}$$

Assuming a homogenous radial distribution of dopant in the core and the presence of background loss in the EDHFA the rate equation for two level system changes as follows [28]:

$$\frac{dP_P(z)}{dz} = -2\pi\sigma_a^P N_0 \times \int_0^\rho \left( \frac{1 + \frac{\eta_s}{1+\eta_s}\frac{P_S(z)\psi_S(r)}{I_{SO}}}{1 + \frac{P_P(z)\psi_P(r)}{I_{PO}} + \frac{P_S(z)\psi_S(r)}{I_{SO}}} + \frac{\alpha_P}{2\pi\sigma_a^P N_0} \right) P_P(z)\,\psi_P(r)\,r dr \quad (12)$$

$$\frac{dP_S(z)}{dz} = 2\pi\sigma_a^S N_0 \times \int_0^\rho \left( \frac{\eta_s \frac{P_P(z)\psi_P(r)}{I_{PO}} - 1}{1 + \frac{P_P(z)\psi_P(r)}{I_{PO}} + \frac{P_S(z)\psi_S(r)}{I_{SO}}} - \frac{\alpha_S}{2\pi\sigma_a^s N_0} \right) P_S(z)\,\psi_S(r)\,r dr \quad (13)$$

where $P_p$ and $P_s$ are pump and signal powers along the propagation length, $\sigma_a^s$, $\sigma_a^p$, and $\sigma_e^s$ are absorption cross-sections of signal and pump, and emission cross-section of signal respectively, $\tau$ is steady-state lifetime, $\Psi_p$, $\Psi_s$ are the qualitative patterns of the pumping and signal propagations, considered as Gaussian envelopes, $\alpha_p$ and $\alpha_s$ are background loss coefficients at pump and signal wavelengths, respectively, $\eta = \sigma_e^s/\sigma_a^s$, and $N_0$ is Erbium concentration in ion/m$^3$ The signal $I_{s0}$ and pumping $I_{p0}$ saturation intensities are defined as:

$$I_{S0} = \frac{h\nu_s}{\sigma_a^s \tau\,(1+\eta_s)}, \quad I_{P0} = \frac{h\nu_p}{\sigma_a^p \tau} \quad (14)$$

where $\nu_s$ and $\nu_p$ are signal and pump frequencies respectively, $h$ is Planck's constant. By numerical solution of Eqs. (12) and (13) the variations of pump and signal along the EDHFA is obtained. In the present paper to solve Eqs. (12) and (13), we have used Runge-Kutta method [29].

## 3. SIMULATION RESULTS AND DISCUSSIONS

The refractive index of glass at 1530 and 980 nm for $x = 0$, using Eq. (9) are 1.4534 and 1.4487, respectively and for glass doped with 6% mole $GeO_2$, are 1.4524 and 1.4575 respectively. Meanwhile, we assume that the Erbium ions do not alter the refractive index of the core. Using Eq. (2) the value of $n_{FSM}$ or refractive index of cladding is obtained. The simulation results of $n_{FSM\,(S)}$ and $n_{FSM\,(P)}$ in terms of AFF $d/\Lambda$ are depicted in Figs. 3(a) and 3(b) for different $\Lambda$ at signal and pump wavelengths, respectively As depicted in Fig. 3, for larger AFF with constant pitch size, the value of $n_{FSM}$ is smaller, because in

larger AHS the cladding has lager area of air filling and the refractive index of cladding is closer to refractive index of air. At a given AFF, if the space between air-hole becomes larger, area of cladding has more silica material so the refractive index of cladding must be closer to the silica refractive index. As shown in Fig. 3, when $\Lambda$ increases, the value of $n_{FSM}$ will increase to a constant value of 1.45 and at lower values of $\Lambda$, the slope of $n_{FSM}$ variations increases. This case occurs at both the wavelengths.

Using Eq. (8), the value of $n_{eff}$ is obtained. The result of simulation for $n_{eff}$ at signal and pump wavelengths by varying AFF and the space between air-holes are depicted in Figs. 4(a) and 2(b), respectively. The value of $n_{eff}$ for $\Lambda$ from 3 to 8 µm is almost

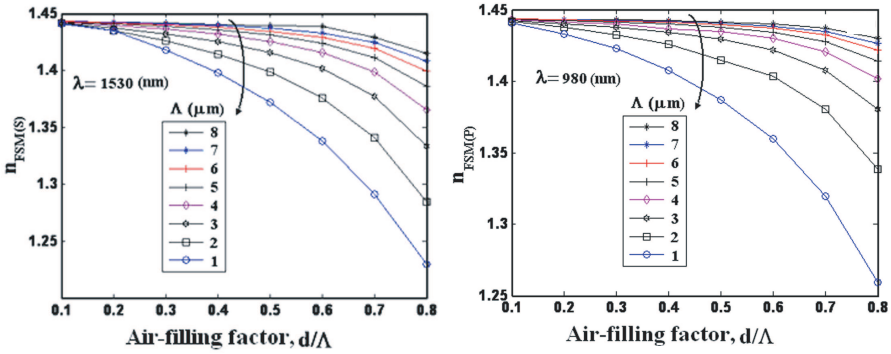


(a) (b)

**Figure 3.** Variation of (a) $n_{FSM(S)}$ at signal wavelength and (b) $n_{FSM(P)}$ at pump wavelength 980 nm versus AFF $d/\Lambda$ for different $\Lambda$.

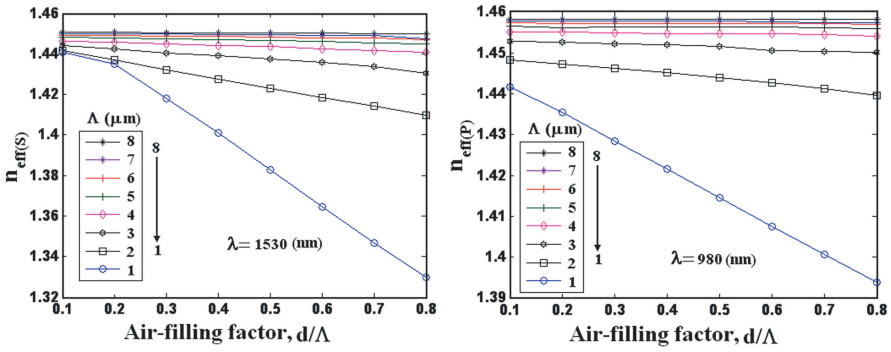


(a) (b)

**Figure 4.** Variations of (a) $n_{FSM(S)}$ at signal wavelength 1530 nm and (b) $n_{FSM(P)}$ pump wavelength 980 nm versus $d/\Lambda$.

independent of AHS variations. At 1530 nm for $\Lambda = 1\,\mu$m, when AFF changes from 0.1 to 0.8, the value of $n_{eff}$ decreases from 1.44 to 1.33. Same as the $n_{FSM}$, the $n_{eff}$ values at 980 nm are larger than that at 1530 nm.

The numerical value of the refractive index using SEIM is higher than the value obtained by FEM [22]. For instance, using SEIM at 1530 nm and $d/\Lambda = 0.1$ and 0.3, the values are 1.4550 and 1.4546, respectively, while FEM yields the respective values as 1.4460 and 1.4447 [18]. For these values of $d/\Lambda$, the relative refractive index difference between the core and cladding using SEIM and FEM are 0.004 and 0.0013, respectively.

The single-mode region in an SIF is determined by its normalized frequency $V = k_0\rho(n_{co}^2 - n_{cl}^2)^{0.5}$ limited to a value of 2.4048. In case of HF, different values of $V$ for the cutoff of single-mode operation depend on definition of core radius $\rho$, refractive indices of the core $n_{co}$ and cladding $n_{cl}$, and the HF description method [30]. To model the HF, for the effective refractive index of the guided principal mode $n_{co}$, with core radii of $\rho = \Lambda/2$, $\rho = \Lambda$, and $\rho = \Lambda/\sqrt{3}$, the effective cutoff values of $V_{eff}$ are obtained as 2.5, $\pi$, and 2.405, using full-vectorial plane-wave expansion method [31], effective-index method [32], and classical optical fiber theories [33]. Although all these methods are shown to be capable of properly describing the behavior of the HFs for at least the simplest cases, they result in different values of the single-mode cutoff values of $V_{eff}$. In all the reported results, the values of $V_{eff}$ depends on $\Lambda/\lambda$ and the HFs stand single-mode in wide range of wavelength.

The variation of $V_{eff}$ with respect to the AFF at signal wavelength for different $\Lambda$ size is illustrated in Fig. 5. For $V_{eff\text{-}SM} < 2.4048$, the HF at 1530 nm for about $\Lambda < 5\,\mu$m can act as single-mode, as shown in Fig. 5(a) by solid line and in Fig. 5(b) by constant plane P. As reported in Ref. [16], the HF made from pure silica without doping of core region with $\Lambda = 2.3\,\mu$m and core radius $\rho = \Lambda/\sqrt{3}$, the maximum value of $d/\Lambda$, for which HF remains single-mode, equals to 0.424 for all wavelengths. Increase in core radius shifts the single-mode region to shorter $d/\Lambda$ values [34]. Simulation shows increasing 6% Ge in the core region with the same $\Lambda = 2.3\,\mu$m causes the maximum value of $d/\Lambda$ increase to 0.536 for which HF remains single-mode.

In the single-mode region of the HF for $V_{eff} < 2.4048$, the maximum value of the pitch $\Lambda$ varies with AFF $d/\Lambda$ at signal and pump wavelengths, as plotted in Fig. 6. For drawing this variation at every value of $d/\Lambda$, the pitch size from Fig. 5(a) is calculated to get $V_{eff} = 2.4048$ for a HF with core radius $\rho = 0.64\Lambda$. The areas under two curves (regions I and II) in Fig. 6 are single-mode

regions for both signal and pump wavelengths. At signal wavelength for $d/\Lambda = 0.1$, pitch $\Lambda$ can grow up to the maximum value of 5.3 µm, where the EDHFA remain single-mode. At larger AFFs, the maximum value of pitch, at which the EDHFA remains single-mode, becomes smaller. Meanwhile, at pump wavelength for $d/\Lambda = 0.1$, for single-mode operation of the EDHFA, pitch attains a maximum value of 2.75 µm. To achieve maximum efficiency of pump and signal, the EDHFA should be single-mode for both the wavelengths. The region common to both the curves (region III) is single-mode region for both signal and pump wavelengths. If the HF used for a design of amplifier or laser for a wideband applications such as wavelength division multiplexers (WDMs), it should remain single-mode for higher gain at all signal wavelengths.

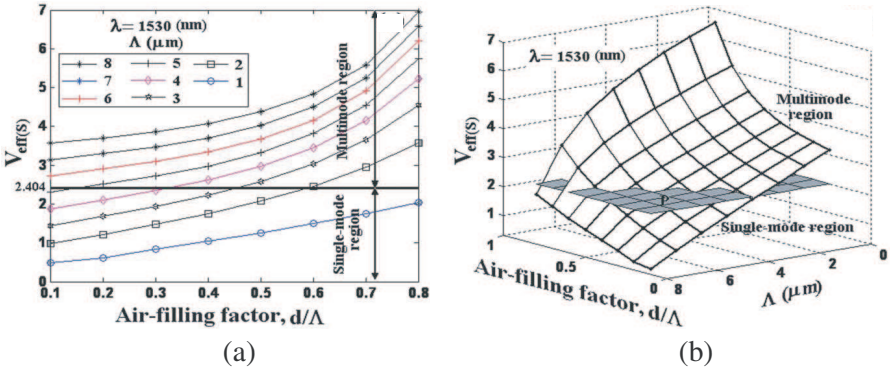


**Figure 5.** Variation of $V_{eff}$ with AFF $d/\Lambda$ for different $\Lambda$ at 1530 nm.

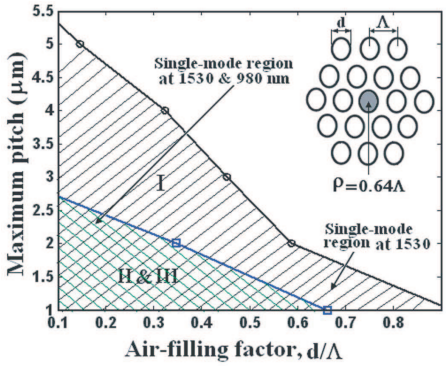


**Figure 6.** Single-mode region of the EDHF for pump and signal wavelengths.

Another parameter, which is influenced by the HF geometry at signal and pump wavelengths, is the effective MFD $\Omega_{eff}$ of the principle mode $LP_{01}$ based on Eq. (11). The variations of $\Omega_{eff}$ at signal $\Omega_s$ and pump $\Omega_p$ wavelengths as functions of the AFF at different values of the pitch, are shown in Figs. 7(a) and 7(b), respectively. For any pitch value when AFF increases, the values of $\Omega_s$ and $\Omega_p$ will decrease. At a constant AFF, growth in air-hole spacing $\Lambda$ causes the MFD to increase both at signal and pump wavelengths. The values of $\Omega_p$ for $\Lambda > 3\,\mu m$ are slightly greater than that of $\Omega_s$ values. The slope of signal MFD reduction for $\Lambda < 3\,\mu m$ becomes steeper as $d/\Lambda$ increases.

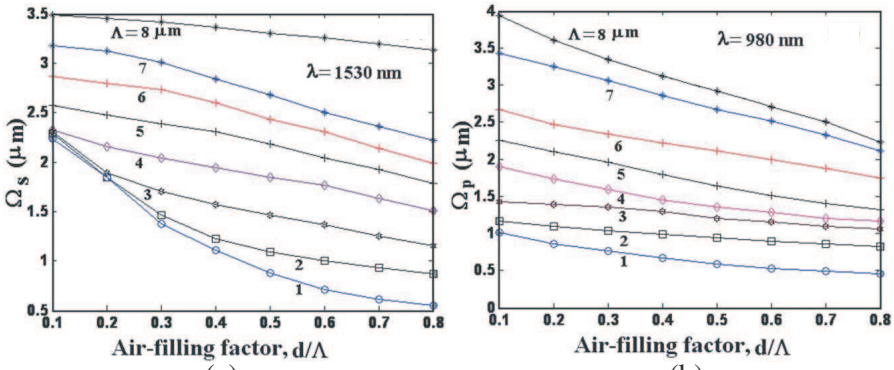


**Figure 7.** Variation of mode field diameter with respect to $d/\Lambda$ for different pitch values at (a) signal wavelength and (b) pump wavelength.

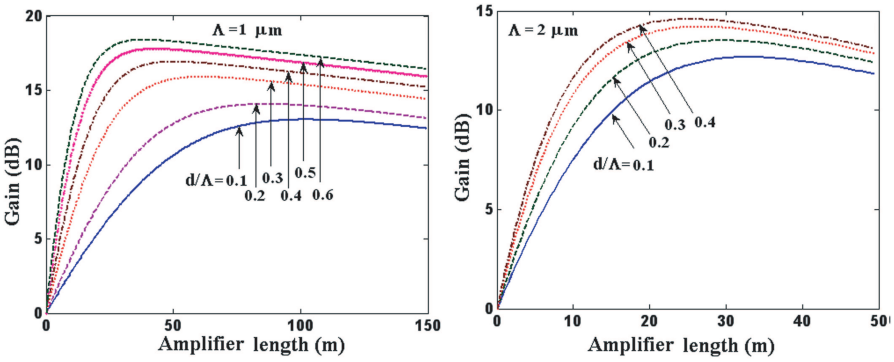


**Figure 8.** Gain variations of EDHFA with respect to amplifier length at different values of $d/\Lambda$ for (a) $\Lambda = 1$ and (b) $\Lambda = 2$.

**Table 1.** Parameters values used in simulation of EDHFAs and EDFAs.

| **Parameters** | **Values** |
|---|---|
| Core diameter of the HF | $\rho = 0.64\Lambda$ |
| Signal wavelength | $\lambda_s = 1530\,\text{nm}$ |
| Pump wavelength | $\lambda_p = 980\,\text{nm}$ |
| Steady-state lifetime | $\text{T} = 10\,\text{ms}$ |
| Dopant concentration | $N_t = 2 \times 10^{24}\,\text{ion/m}^3$ |
| Pump absorption cross section [35] | $\sigma_p^a = 1.6400 \times 10^{-25}\,\text{m}^2$ |
| Signal absorption cross section [35] | $\sigma_s^a = 2.4249 \times 10^{-25}\,\text{m}^2$ |
| Signal emission cross section [35] | $\sigma_s^e = 2.4097 \times 10^{-25}\,\text{m}^2$ |
| Input pump power | $P_p = 6\,\text{mW}$ |
| Input signal power | $P_s = 1\,\text{mW}$ |
| Signal background loss | $\alpha_S = 0.41\,\text{dB/km}$ [18] |
| Pump background loss | $\alpha_P = 2\,\text{dB/km}$ [18] |

By numerically solving Eqs. (12) and (13) in single-mode region of Fig. 6, using Runge-Kutta method, the gain variation along the length of EDHFA is obtained as shown in Figs. 8(a) and 8(b) for $\Lambda = 1\,\mu\text{m}$ and $2\,\mu\text{m}$ at different AFF, respectively. It is noted that in both values of $\Lambda$, increase in the AFF will make the maximum gain increase and the optimum length of EDHFA decrease. In these simulations, we used the values of main parameters such as dopant concentration, steady-state lifetime, cross-sections, signal and pump values from Table 1 [35]. As shown in Fig. 8(b) the optimum length is shorter for when $\Lambda = 2\,\mu\text{m}$, so the use of $\Lambda = 2\,\mu\text{m}$ to achieve shorter amplifier length is preferred. For instance, in [18], at $\Lambda = 4\,\mu\text{m}$ and $d/\Lambda = 0.25$ for signal power of 1 mW and pump power of 10 mW, the gain at the length of 13 m is 7.6 dB whereas in the present result at $\Lambda = 2\,\mu\text{m}$ and $d/\Lambda = 0.1$ for signal power of 1 mW and pump power of 6 mW, we obtained a gain of 9.1 dB with the same length. The higher gain in the later case could be due to the use of pumping wavelength within single-mode region of the EDHFA.

To visualize the maximum gain variations and the optimum length of the amplifier with respect to the AFF and $\Lambda$ as a parameter, we have illustrated their variations in Figs. 9(a) and 9(b) for the pump and the signal wavelengths of $980\,\mu\text{m}$ and $1530\,\mu\text{m}$, respectively. The maximum gain of the amplifier in the single-mode region of the HF down-shifts to lower values in terms of $\Lambda$ and for $d/\Lambda$ up to 0.2, and the slope of the maximum gain variation for both values of $\Lambda$ remains the same. When $d/\Lambda > 0.2$, effect of $\Lambda$ becomes more prominent.

When the AFF increases, the maximum gain will also increase while the optimum length will decrease. It is obvious to see the reduction of optimum length of about 75% when $\Lambda$ increases. So by choice of proper HF geometry we can achieve higher gain at shorter amplifier length.

The variations of maximum gain and optimum length with respect to pump power at $\Lambda = 2\,\mu m$ and $N_t = 2.0 \times 10^{24}$ ion/m$^3$ for different values of $d/\Lambda$ are depicted in Figs. 10(a) and 10(b), respectively. The variations of both the parameters have ascending order as that of Ref. [18].

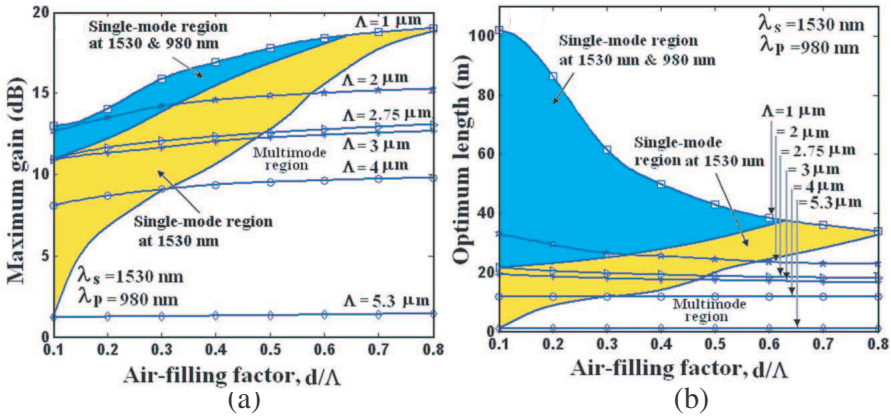


**Figure 9.** (a) Maximum gain variation and (b) optimum length with respect to AFF at $\Lambda = 1\,\mu m$ and $2\,\mu m$ in single-mode region of the HF.

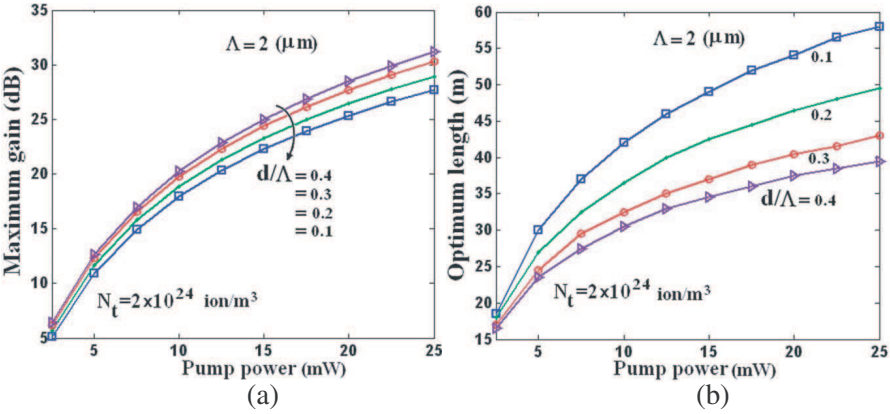


**Figure 10.** (a) Maximum gain, (b) optimum length variation with respect to pump power at $\Lambda = 2\,\mu m$ and different AFF.

Similar to conventional EDFA, when pump power increases, the maximum gain and optimum length will increase, as shown in Fig. 10(a). For 25 mW pump power, the variance between maximum gain at $d/\Lambda = 0.1$ and 0.4 is about 5 dB and the difference between optimum length for the same AFF is about 29 m. We note that in Fig. 10(b), when $d/\Lambda$ increases, the optimum length will decrease, and the gain will increase, especially at higher pump powers. So using higher value of AFF in designing amplifier at high pump power will be more detrimental issue. Further another feature of shorter amplifier lengths is the less effect of amplified spontaneous emission (ASE) on its performance [36, 37]. In a comparison of the EDHFA with conventional EDFA, the variation of pump power or signal power or distribution of dopant concentration has similar effect on the performance of the amplifiers. In other words, increase of the pump power or dopant concentration and/or decrease of the signal power cause an increase of the gain of the EDHFA along a constant length of the amplifier [18], as similar to EDFA [27].

The variations of maximum gain and optimum length with respect to dopant concentration are depicted in Fig. 11. As shown in Fig. 11(a), increases in dopant concentration gradually causes increases in the maximum gain. Similar to Fig. (9), the values of maximum gain at a larger AFF is higher. The dopant concentration in a fixed amplifier length in excess of $2.0 \times 10^{24}$ ion/m$^3$ will lower down the gain [38] because higher $Er^{3+}$ concentration worsens the amplifier performance due to pair-induced quenching (PIQ) which appears in a conventional EDFA [39]. So by changing hole geometry rather than increasing the dopant concentration, we can get higher gain value and omit the undesirable effects such as PIQ.

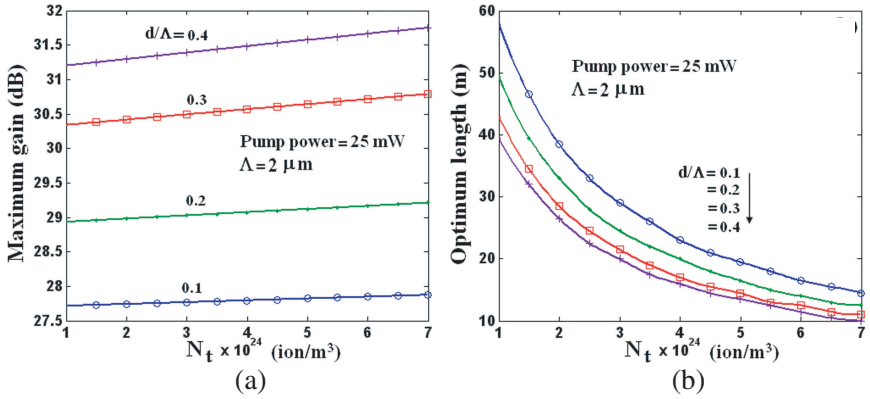


**Figure 11.** Variations of (a) maximum gain and (b) optimum length with respect to dopant concentration at $\Lambda = 2\,\mu$m and different AFFs.

As shown in Fig. 11(b) when the dopant concentration is $1.0 \times 10^{24}$ ion/m$^3$, the optimum length changes from 30 m to 55 m for different AFFs. By increase of the dopant concentration up to $7.0 \times 10^{24}$ ion/m$^3$, the optimum length decreases to 7.3–13.3 m. Similar to Ref. [18], we note in Fig. 11(b) that the length of EDHF has a reduction trend when the dopant concentration increases.

As shown in Fig. 9(b), using hole geometry with $\Lambda = 1\,\mu$m causes the optimum length shifts to higher length. So use of $\Lambda = 1\,\mu$m is not preferred. As shown in Fig. 11(b), the optimum lengths after $N_t = 3.0 \times 10^{24}$ ion/m$^3$ for different $d/\Lambda$ have mild slope change. In addition, from Fig. 11(a), we observe that the maximum gains for this case vary with negligible change. So the best value for dopant concentration could be about $3.0 \times 10^{24}$ ion/m$^3$ which gives a benefit of avoiding the upconversion and QIP effects in the amplifier of the kind under consideration.

In the following, we analytically compare the result of amplifier gain using FEM and SEIM methods.

In Ref. [25], the effective indices obtained by FEM and SEIM at 1500 and 1000 nm are presented. Using Eqs. (6) and (11) and Figs. 4 and 5 of Ref. [25], the MFD can be obtained approximately at given wavelengths.

Using the obtained MFDs in Eqs. (12) and (13), the gain values can be calculated. The gain variations with respect to amplifier length at 1500, 1530 and 1550 nm are depicted in Fig. 12 using the values of amplifier parameters from Table 1. We note that the difference between maximum gain at 1550 nm, 1530 nm, and 1500 nm are 0.54 dB, 0.17 dB and 2.67 dB, respectively. The corresponding optimum lengths are 7.8 m, 11.3 m, and more than 23 m.

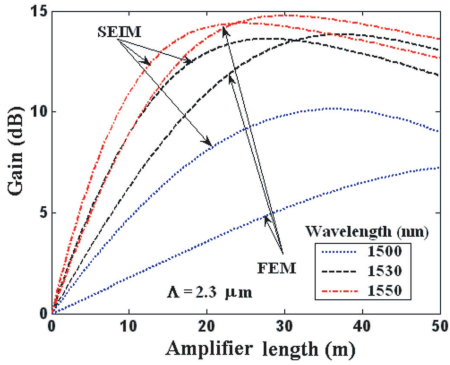


**Figure 12.** Variation of amplifier gain with respect to amplifier length at 1500, 1530 and 1550 nm.

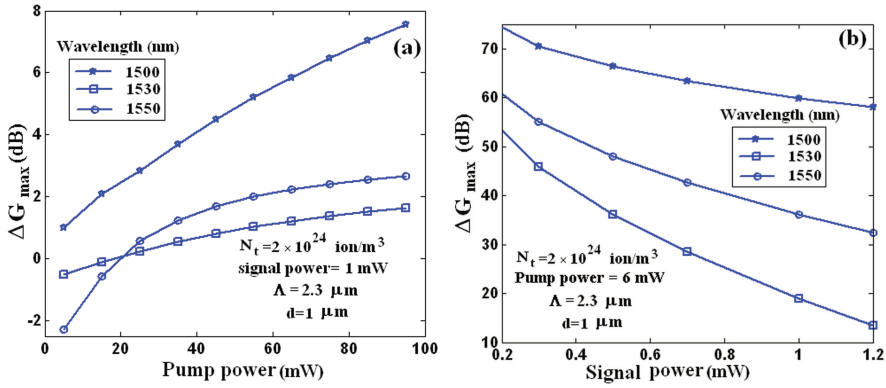


**Figure 13.** Maximum gain difference obtained by FEM and SEIM as a function of pump power.

The difference between amplifier parameters from FEM and SEIM depends on the pump and signal input powers. The maximum gain difference between two methods as $\Delta G_{\max}(= G_{\max(SEIM)} - G_{\max(FEM)})$ is shown in Figs. 13(a) and 13(b), respectively, for pump and input powers at wavelengths 1500 nm, 1530 nm, and 1550 nm, $\Lambda = 2.3\,\mu$m, and $d = 1\,\mu$m. We note that when the pump power increases, the $\Delta G_{\max}$ value also increases. However, when the input signal power decreases, the value of $\Delta G_{\max}$ would increase.

## 4. CONCLUSION

In this paper, Erbium doped holey fiber amplifiers are analyzed using scalar effective index method. The variations of $n_{eff}$, $n_{FSM}$, for different values of AHSs and AFFs are obtained. Simulation shows that both the refractive indices $n_{eff}$ and $n_{FSM}$ are functions of $d/\Lambda$ and the pitch $\Lambda$ at signal and pump wavelengths. At the both wavelengths, the indices for higher $\Lambda$ have higher values in terms of $d/\Lambda$.

It is shown that with variations of AHS and AFF, one can design an amplifier in such a way that for both signal and pump wavelengths the single-mode operation is maintained for enhancement of the gain.

It is shown that single-mode region of the HF increases almost linearly with respect to $d/\Lambda$ and $\Lambda$. For a single-mode operation of EDHFA, when $d/\Lambda = 0.1$, the pitch $\Lambda$ can reach to a maximum value of 5.3 μm at signal wavelength with 6% Ge doped core. At larger $d/\Lambda$, the maximum value of pitch, at which the EDHFA remains single-mode, becomes smaller. In case of pump wavelength, the maximum value of $\Lambda$ is about 2.75 μm for the same value of $d/\Lambda$. To achieve

maximum efficiency the EDHFA must be single-moded at signal and pump wavelengths.

The mode field diameter of the EDHFA is another parameter that is influenced by $d/\Lambda$ and $\Lambda$. At pump wavelength, the effect on the MFD is more at higher values of $\Lambda$ while for signal wavelength, the effect is more prominent at lower $\Lambda$.

The maximum gain and the optimum length of EDHFA at single-mode region at 6 mW pump power and 1 mW signal power, are depicted. It is shown that for larger $d/\Lambda$ the value of maximum gain is greater and the optimum length becomes shorter. So use of larger $d/\Lambda$ in designing amplifier is recommended. When $d/\Lambda$ increases, the gain also increases with decrease of the pitch $\Lambda$.

Simulation shows by increasing dopant concentration, the value of maximum gain increases whereas the optimum length decreases. The gain has higher value at larger AFF. So using larger AFF can yield shorter amplifier length with higher gain without requiring of increase in dopant concentration. So using HF to design fiber amplifier can decrease undesired effects such as nonlinear effect and PIQ.

Increase in pump power causes increase in both maximum gain and optimum length. For 25 mW pump power the difference between the maximum gain at $d/\Lambda = 0.1$ and 0.4 is about 5 dB, and the difference between optimum length with the same AFF is about 29 m. Therefore, use of larger AFF at high pump power can reduce the amplifier length.

A qualitative comparison shows that at wavelength 1500 nm, among other two wavelengths 1530 nm, and 1550 nm, the gain of the amplifier obtained by FEM and SEIM has more difference. In addition, it is shown that the differences in results of two methods would increase by pump and input powers.

Although the analysis via FEM is more accurate, it is a time-consuming method for analysis of geometrical effects on amplification characteristics of the EDHFA. Meanwhile, it is shown that the SEIM analysis can predict suitably the effects of wide range of geometrical changes of the HF on the amplifier performance.

## REFERENCES

1. Russell, P., "Photonic crystal fibers," *Science*, Vol. 299, 358–362, 2003.
2. Midrio, M., M. P. Singh, and C. G. Someda, "The space filling mode of holey fibers: An analytical vectorial solution," *IEEE J. Ligthwave Technol.*, Vol. 18, 1031–1037, 2000.
3. Bjarklev, A., J. Broeng, and A. S. Bjarklev, *Photonic Crystal Fibers*, Kluwer Academic Publishers, London, 2003.

4. Peucheret, C., B. Zsigri, P. A. Andersen, K. S. Berg, A. Tersigni, P. Jeppesen, K. P. Hansen, and M. D. Nielsen, "40 Gbit/s transmission over photonic crystal fibre using mid-span spectral inversion in highly nonlinear photonic crystal fibre," *Electron. Lett.*, Vol. 39, No. 12, 919–921, 2003.
5. Zsigri, B., C. Peucheret, M. D. Nielsen, and P. Jeppesen, "Transmission over 5.6 km large effective area and low-loss (1.7 dB/km) photonic crystal fibre," *Electron. Lett.*, Vol. 39, No. 10, 796–798, 2003.
6. Benabid, F., J. C. Knight, G. Antonopoulos, and P. S. J. Russell, "Stimulated Raman scattering in hydrogen-filled hollow-core photonic crystal fiber," *Science*, Vol. 298, No. 5592, 399–402, 2002.
7. Monro, T. M., W. Belardi, K. Furusawa, J. C. Baggett, N. G. R. Broderick, and D. J. Richardson, "Sensing with microstructured optical fibres," *Meas. Sci. Technol.*, Vol. 12, 854–858, 2001.
8. Limpert, J., T. Schreiber, S. Nolte, H. Zellmer, A. Tünnermann, R. Iliew, F. Lederer, J. Broeng, G. Vienne, A. Petersson, and C. Jakobsen, "High-power air-clad large-mode-area photonic crystal fiber laser," *Opt. Express*, Vol. 11, 818–823, 2003.
9. Hansen, K. P., "Dispersion flattened hybrid-core nonlinear photonic crystal fiber," *Opt. Express*, Vol. 11, 1503–1509, 2003.
10. Diddams, S. A., D. J. Jones, J. Ye, S. T. Cundiff, J. L. Hall, J. K. Ranka, R. S. Windeler, R. Holzwarth, T. Udem, and T. W. Hänsch, "Direct link between microwave and optical frequencies with a 300 THz femtosecond laser comb," *Phys. Rev. Lett.*, Vol. 84, 5102–5105, 2000.
11. Park, K. N., T. Erdogan, and K. S. Lee, "Cladding mode coupling in long-period gratings formed in photonic crystal fibers," *Opt. Commun.*, Vol. 266, 541–545, 2006.
12. Shirakawa, A., J. Ota, M. Musha, K. Nakagawa, K. Ueda, J. R. Folkenberg, and J. Broeng, "Large-mode-area erbium-ytterbium-doped photonic-crystal fiber amplifier for high-energy femtosecond pulses at 1.55 μm," *Opt. Express*, Vol. 13, 1221–1227, 2005.
13. Genty, G., M. Lehtonen, H. Ludvigsen, J. Broeng, and M. Kaivola, "Spectral broadening of femtosecond pulses into continuum radiation in micro structured fibers," *Opt. Express*, Vol. 10, 1083–1098, 2002.
14. Sharping, J. E., M. Fiorentino, P. Kumar, and R. S. Windeler, "Optical parametric oscillator based on four-wave mixing in microstructure fiber," *Opt. Lett.*, Vol. 27, 1675–1677, 2002.

15. Nielsen, M. D., C. Jacobsen, N. A. Mortensen, J. R. Folkenberg, and H. R. Simonsen, "Low-loss photonic crystal fibers for transmission systems and their dispersion properties," *Opt. Express*, Vol. 12, 1372–1376, 2004.
16. Kunimasa, S. and K. Masanori, "Numerical modeling of photonic crystal fibers," *IEEE J. Ligthwave Technol.*, Vol. 23, 3580–3590, 2005.
17. Seraji, F. E. and M. D. Talebzadeh, "Analysis of erbium doped holey fiber using fundamental space filling mode," *Chin. Opt. Lett.*, Vol. 6, 644–647, 2008.
18. Prudenzano, F., "Erbium-doped hole-assisted optical fiber amplifier: Design and optimization," *IEEE J. Ligthwave Technol.*, Vol. 23, 330–340, 2005.
19. Cucinotta, A., F. Poli, S. Selleri, L. Vincetti, and M. Zoboli, "Amplification properties of $Er^{3+}$-doped photonic crystal fibers," *IEEE J. Ligthwave Technol.*, Vol. 21, 782–788, 2003.
20. Poli, F., A. Cucinotta, D. Passaro, S. Selleri, J. Lægsgaard, and J. Broeng, "Single-mode regime in large-mode-area rare-earth-doped rod-type PCFs," *IEEE J. Select. Topic. Quant. Electron.*, Vol. 15, 54–60, 2009.
21. Furusawa, K., T. Kogure, T. M. Monro, and D. J. Richardson, "High gain efficiency amplifier based on an erbium doped aluminosilicate holey fiber," *Opt. Express*, Vol. 44, 3452–3458, 2004.
22. Li, Y. F., C. Y. Wang, and M. L. Hu, "A fully vectorial effective index method for photonic crystal fibers: Application to dispersion calculation," *Opt. Commun.*, Vol. 238, 29–33, 2004.
23. Seraji, F. E., M. Rashidi, and M. Karimi, "Characteristics of holey fibers fabricated at different drawing speeds," *Chin. Opt. Lett.*, Vol. 5, 131–134, 2007.
24. Varshney, S. K., M. P. Singh, and R. K. Sinha, "Propagation characteristics of photonic crystal fibers," *Opt. Commun.*, Vol. 24, 192–198, 2003.
25. Li, Y. F., C. Y. Wang, Z. H. Wang, M. L. Hu, and L. Chai, "Analytical solution of the fundamental space filling mode of photonic crystal fibers," *Opt. Laser Technol.*, Vol. 39, 322–326, 2007.
26. Midrio, M., M. P. Singh, and C. G. Someda, "The space filling mode of holey fibers: An analytical vectorial solution," *IEEE J. Ligthwave Technol.*, Vol. 18, 1031–1037, 2000.
27. Desurvire, E., *Erbium Doped Fiber Amplifiers: Principles and*

*Applications*, Wiley, New York, 1994.

28. Giles, C. R. and E. Desurvire, "Modeling erbium-doped fiber amplifiers," *IEEE. J. Lightwave Technol.*, Vol. 9, 271, 1991.
29. Mathews, J. H. and K. K. Fink, *Numerical Methods Using Matlab*, 4th Edition, Prentice-Hall Inc., 2004.
30. Li, H., A. Mafi, A. Schülzgen, L. Li, V. L. Temyanko, N. Peyghambarian, and J. V. Moloney, "Analysis and design of photonic crystal fibers based on an improved effective-index method," *IEEE J. Ligthwave Technol.*, Vol. 25, 1224–1230, 2007.
31. Broeng, J., D. Mogilevstev, S. E. Barkou, and A. Bjarklev, "Photonic crystal fibers: A new class of optical waveguides," *Opt. Fiber Technol.*, Vol. 5, 305–330, 1999.
32. Mortensen, N. A., J. R. Folkenberg, M. D. Nielsen, and K. P. Hansen, "Modal cutoff and the $V$ parameter in photonic crystal fibers," *Opt. Lett.*, Vol. 28, 1879–1881, 2003.
33. Koshiba, M. and K. Saitoh, "Applicability of classical optical fiber theories to holey fibers," *Opt. Lett.*, Vol. 29, 1739–1741, 2004.
34. Saitoh, K., Y. Tsuchida, and M. Koshiba, N. A. Mortensen, "Endlessly single-mode holey fibers: The influence of core design," *Opt. Express*, Vol. 13, 10833–10839, 2005.
35. Barnes, W. L., R. I. Laming, E. J. Tarbox, and P. R. Morkel, "Absorption and emission cross sections of $Er^{3+}$ doped silica fibers," *IEEE J. Quant. Electron.*, Vol. 27, 1004–1010, 1991.
36. Desurvire, E. and J. Simpson, "Amplification of spontaneous emission in erbium-doped single-mode fibers," *IEEE J. Ligthwave Technol.*, Vol. 7, 835–845, 1989.
37. Becker, P. C., N. A. Olsson, and J. R. Simpson, *Erbium Doped Fiber Amplifiers Fundamentals and Technology*, Academic Press, London, 1999.
38. D'Orazio, A., M. de Sario, L. Mescia, and V. Petruzzelli, and F. Prudenzano, "Refinement of $Er^{3+}$-doped hole-assisted optical fiber amplifier," *Opt. Express*, Vol. 13, No. 25, 9970–9981, 2005.
39. Myslinsky, P., D. Nguyen, and J. Chrostowski, "Effects of concentration on the performance of erbiumdoped fiber amplifiers," *IEEE J. Lightwave Technol.*, Vol. 15, 112–120, 1997.